Spectroscopy of f-f transitions, crystal-field calculations, and magnetic and quadrupole helix chirality in $DyFe_3(BO_3)_4$

M. N. Popova, E. P. Chukalina, and K. N. Boldyrev*
Institute of Spectroscopy, Russian Academy of Sciences, 108840 Moscow, Troitsk, Russia

T. N. Stanislavchuk
Department of Physics, New Jersey Institute of Technology, Newark, New Jersey 07102, USA

B. Z. Malkin
Kazan Federal University, 420008 Kazan, Russia

I. A. Gudim
Kirensky Institute of Physics, Siberian Branch of RAS, 660036 Krasnoyarsk, Russia

(Received 24 November 2016; revised manuscript received 5 February 2017; published 27 March 2017)

We present the results of temperature- and polarization-dependent high-resolution optical spectroscopy studies of $DyFe_3(BO_3)_4$ performed in spectral ranges $40-300\,cm^{-1}$ and $3000-23\,000\,cm^{-1}$. The crystal-field (CF) parameters for the Dy^{3+} ions in the $P3_121$ ($P3_221$) phase of $DyFe_3(BO_3)_4$ are obtained from calculations based on the analysis of the measured f-f transitions. Recently, quadrupole helix chirality and its domain structure was observed in resonant x-ray diffraction experiments on $DyFe_3(BO_3)_4$ using circularly polarized x rays [T. Usui, Y. Tanaka, H. Nakajima, M. Taguchi, A. Chainani, M. Oura, S. Shin, N. Katayama, H. Sawa, Y. Wakabayashi, and T. Kimura, Nat. Mater. **13**, 611 (2014)]. Using the obtained set of the CF parameters, we calculate temperature dependencies of the electronic quadrupole moments of the Dy^{3+} ions induced by the low-symmetry (C_2) CF component and show that the quadrupole helix chirality can be explained quantitatively. We also consider the temperature dependencies of the bulk magnetic dc-susceptibility and the helix chirality of the single-site magnetic susceptibility tensors of the Dy^{3+} ions in the paramagnetic $P3_121$ ($P3_221$) phase and suggest the neutron and resonant x-ray diffraction experiments in a magnetic field to reveal the helix chirality of field-induced magnetic moments.

DOI: 10.1103/PhysRevB.95.125131

I. INTRODUCTION

Chirality, or handedness, is the asymmetry of an object upon its mirroring. In crystals, chirality can be connected with a helical crystal structure, which gives rise to such functionality as optical rotatory power [1]. Magnetic chirality corresponding to twisted magnetic structures induces ferroelectricity in a number of multiferroics [2]. Recent work [3] has introduced a new concept of "chirality of electronic quadrupole moments" on the basis of resonant x-ray diffraction (RXD) studies using circularly polarized x rays, which may lead to a new material functionality. In Ref. [3], single-crystal specimens of $DyFe_3(BO_3)_4$ were employed.

The $DyFe_3(BO_3)_4$ crystals belong to the borate family with general formula $RM_3(BO_3)_4$, where R is a rare earth (RE) or Y ion but M = Al, Ga, Sc, Fe, or Cr. These compounds crystallize in the trigonal $R32$ structure of the natural mineral huntite [4]. The most known representatives of this family are aluminum borates, which are used in self-frequency doubling and self-frequency summing lasers (see, e.g., Refs. [5–7] and references therein). Additional interest of scientists in the huntite borates is connected with an appreciable magnetoelectric effect found in the yttrium and RE iron borates (see, e.g., Refs. [8–11] and references therein) and in the RE aluminum and gallium borates [12–15].

With decreasing the temperature, the iron borates with R = Eu-Er and Y undergo a structural phase transition from the $R32$ (D_3^7, No. 155) phase to a less symmetric but also trigonal one [16–18], corresponding to the enantiomorphic space-group pair $P3_121$ (D_3^4, No. 152) and $P3_221$ (D_3^6, No. 154). Structural motifs showing a difference between these two groups are presented in Fig. 1. The RXD experiments on single-crystal samples of $DyFe_3(BO_3)_4$ [3] revealed macroscopic domains with (sub)millimeter dimensions, which differ by right-handed ($P3_121$) or left-handed ($P3_221$) helical structures of electronic quadrupole moments of the Dy^{3+} ions at temperatures below the structural transition temperature $T_S = 285\,K$ [3]. The domain pattern is robust against temperature cycling across T_S. This is because the high-temperature crystallographic structure ($R32$) is already chiral so that both left- and right-handed crystallographic domains containing left- and right-handed helix chains of FeO_6 octahedra, respectively, already exist above T_S. The quadrupole helix chirality of Dy^{3+} ions develops below T_S (and coexists with the antiferromagnetic order that sets below $T_N = 39\,K$ [19,20]), being closely connected with the crystallographic chirality above T_S. The authors of Ref. [3] conjectured that because of a significant spin-orbit interaction, the direction of a magnetic moment at the Dy site in $DyFe_3(BO_3)_4$ is strongly coupled with the orientation of its electric quadrupole. It is important to note that a multidomain chiral structure may noticeably reduce multiferroic properties of a crystal. It has been found, in particular, that the value of the

*kn.boldyrev@gmail.com

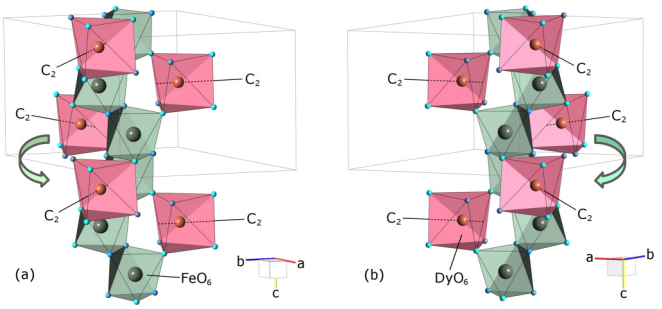

FIG. 1. (a) Left-handed $P3_221$ and (b) right-handed $P3_121$ helical structures of DyO_6 distorted prisms and FeO_6 octahedra in $DyFe_3(BO_3)_4$ crystal at temperatures below the structural transition temperature $T_S = 285$ K. Three crystallographically equivalent but magnetically nonequivalent Dy ions with the local C_2 symmetry are connected by the (a) left-handed and (b) right-handed $(2\pi/3)$ rotations around the c axis.

spontaneous electric polarization observed in $SmFe_3(BO_3)_4$ below T_N appreciably depends on a sample [21]. Control of quadrupole helix chirality using circularly polarized x rays might help to develop growth technologies for obtaining single-domain crystals.

In the present paper, we show that electric quadrupole moments of Dy^{3+} ions in $DyFe_3(BO_3)_4$ are connected with the low-symmetry crystal-field (CF) component that appears below the temperature T_S of the structural phase transition, at which the point symmetry group of the Dy site lowers from D_3 to C_2. A limited availability of experimental data on CF levels of Dy^{3+} ions in $DyFe_3(BO_3)_4$ [22] has prevented a detailed analysis of the electronic density distribution based on the results of CF calculations in the framework of the C_2 symmetry CF Hamiltonian with 15 parameters. In Ref. [23], CF parameters for $DyFe_3(BO_3)_4$ were estimated from the fit to the experimental magnetization data assuming the D_3 symmetry. However, the values and signs of some of these obtained CF parameters contradict to general trends in variations of the CF parameters, even in the RE borates with the $R32$ structure [24–26]. To find reliable CF parameters, we perform a thorough broadband high-resolution optical spectroscopy investigation of the dysprosium iron borate. On the basis of a large set of experimentally found CF energies and preliminary calculations in the framework of the exchange-charge model (ECM) [27], we obtain CF parameters and wave functions of the Dy^{3+} ions in the low-symmetry ($P3_121$ or $P3_221$) phase of $DyFe_3(BO_3)_4$, calculate the electric quadrupole moments, and compare them with those found experimentally in Ref. [3]. We also calculate values of the single-site magnetic susceptibility tensors of the Dy^{3+} ions in the paramagnetic $P3_121$ ($P3_221$) phase, consider the helix chirality of these tensors, and suggest experiments that could bring to light a magnetic chirality in the low-symmetry paramagnetic phase of $DyFe_3(BO_3)_4$.

II. EXPERIMENTAL

Single crystals of dysprosium iron borate were grown on the seeds from solution melts on the basis of $Bi_2Mo_3O_{12}$, as described in Refs. [28] and [29]. To prepare samples for spectroscopic measurements, we cut out 0.2–1.3 mm thick

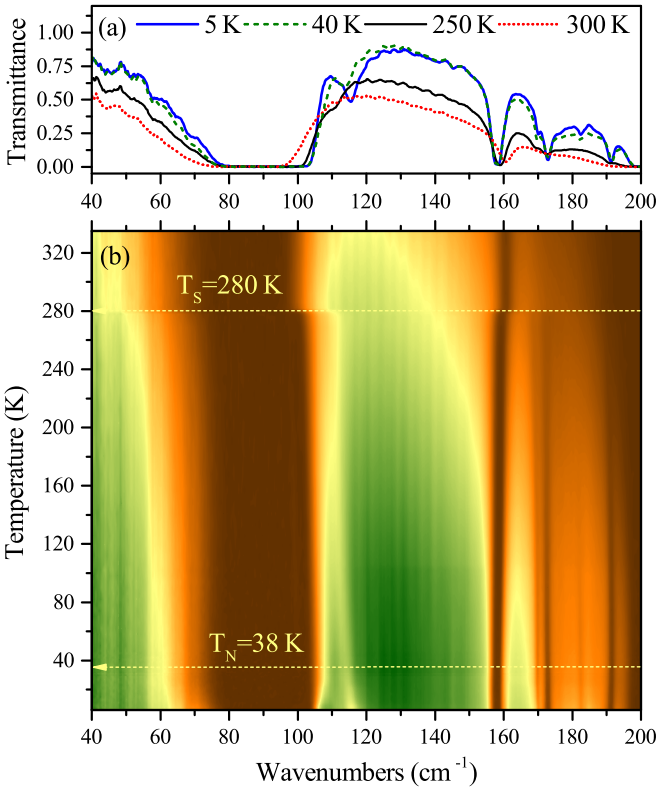

FIG. 2. Far-infrared α-polarized transmission spectra of a $DyFe_3(BO_3)_4$ single crystal (a) at several selected temperatures; (b) presented as intensity maps in the wavenumber–temperature scales.

plates either perpendicular or parallel to the crystallographic c axis of the crystal. Transmission spectra were detected in wide spectral ($3000-23\,000\,cm^{-1}$) and temperature (3.5–300 K) regions using Bruker 125HR and Bomem DA3.002 Fourier spectrometers, with a spectral resolution up to $0.5\,cm^{-1}$. The spectra were measured in different polarizations of the incident radiation, namely, in $\sigma(\boldsymbol{k}\perp c, \boldsymbol{E}\perp c), \pi(\boldsymbol{k}\perp c, \boldsymbol{E}||c)$, and $\alpha(\boldsymbol{k}||c, \boldsymbol{E}, \boldsymbol{H}\perp c)$ polarizations. A very weak optical transition to the $^6F_{1/2}$ level of Dy^{3+} was detected using the thickest available non-oriented sample and nonpolarized light. For cryogenic measurements, we used either an optical helium-vapor cryostat or a closed-cycle Cryomech ST-403 cryostat.

To characterize our samples, we studied their temperature-dependent (10–400 K) polarized infrared vibrational spectra. Being compared with the spectra of $GdFe_3(BO_3)_4$ [30], the crystal structure of which is well known from the temperature-dependent x-ray diffraction studies [16], these spectra unambiguously testify the $R32$ structure at high temperatures, the phase transition into the $P3_121$ ($P3_221$) structure at $T_S = 280$ K, and an absence of any other phases in the samples. Figure 2 shows a part of the far-infrared transmission spectrum of $DyFe_3(BO_3)_4$. An abrupt shift of phonon lines and appearance of new phonons at $T_S = 280$ K are due to a weak first-order structural phase transition [17,30].

In the high-temperature $R32$ structure, the CF of the D_3 symmetry splits multiplets of the Dy^{3+} free ion with the $4f^9$ ground electronic configuration into $(2J+1)/2$ sublevels, where J is the corresponding total half-integer angular

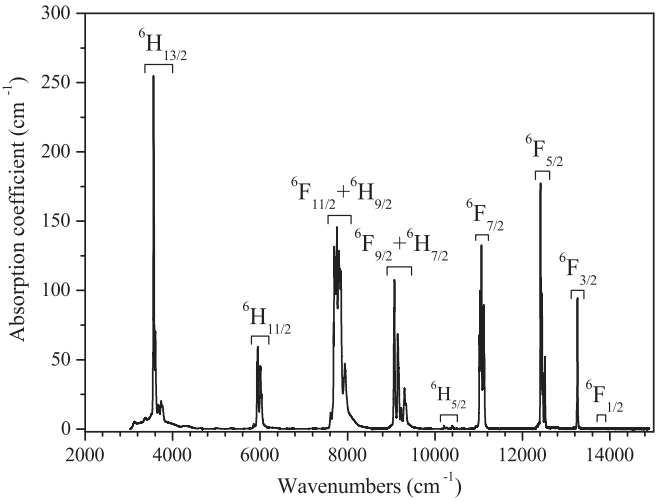

FIG. 3. The σ-polarized absorption spectrum of the Dy^{3+} ions in the dysprosium iron borate at $T = 50$ K.

momentum. Each of these sublevels is doubly degenerated; this Kramers degeneracy can be removed by a magnetic field only. Thus, at the structural phase transition $R32 \rightarrow P3_121$ or $P3_221$, when the symmetry of the Dy^{3+} ion position lowers from D_3 to C_2, all CF sublevels of the Dy^{3+} ion remain doubly degenerated. A magnetic ordering at $T_N = 38$ K was detected from the observed splitting of Kramers doublets in the temperature-dependent electronic spectra of *f-f* transitions of Dy^{3+} in $DyFe_3(BO_3)_4$ (not shown).

III. EXPERIMENTAL RESULTS

In the transmission spectra of RE iron borates, relatively narrow spectral lines corresponding to *f-f* transitions in the RE ions are superimposed onto broad *d-d* bands of the Fe^{3+} ions [24,26]. After subtracting the *d-d* absorption bands [e.g., measured in $GdFe_3(BO_3)_4$, where *f-f* transitions start at energies above $\sim$30 000 cm^{-1}], one gets the spectra of the *f-f* transitions. Figure 3 shows thus obtained absorption spectrum of $DyFe_3(BO_3)_4$ at $T = 50$ K in the spectral range 2000−15 000 cm^{-1}. As one can see in Fig. 3, the first excited multiplet $^6H_{13/2}$ is separated from the lowest multiplet $^6H_{15/2}$ by an energy gap of $\sim$3500 cm^{-1}($\sim$5000 K). Thus, only the CF levels of the multiplet $^6H_{15/2}$ are populated in the studied temperature range (3.5–300 K). Since physical properties of a system are determined by its populated states, data on CF levels of this multiplet are of main interest. Figure 4 presents at expanded scales absorption spectra in the regions of transitions from the multiplet $^6H_{15/2}$ to different excited multiplets of the Dy^{3+} ion. Here and hereafter, notation of a spectral line contains the initial and final levels of an optical transition; CF levels of the lowest multiplet $^6H_{15/2}$ are labeled by numerals and those of a given excited multiplet by capital letters (A, B, etc.). The lines designated 2A, 2B, etc., diminish in intensity with further lowering of the temperature until they completely disappear, while the lines 1A, 1B, etc., which are shifted by 15 cm^{-1} to higher frequencies from the lines 2A, 2B, etc., grow in intensity. Such behavior shows unambiguously that the spectral lines observed at 50 K correspond to the transitions

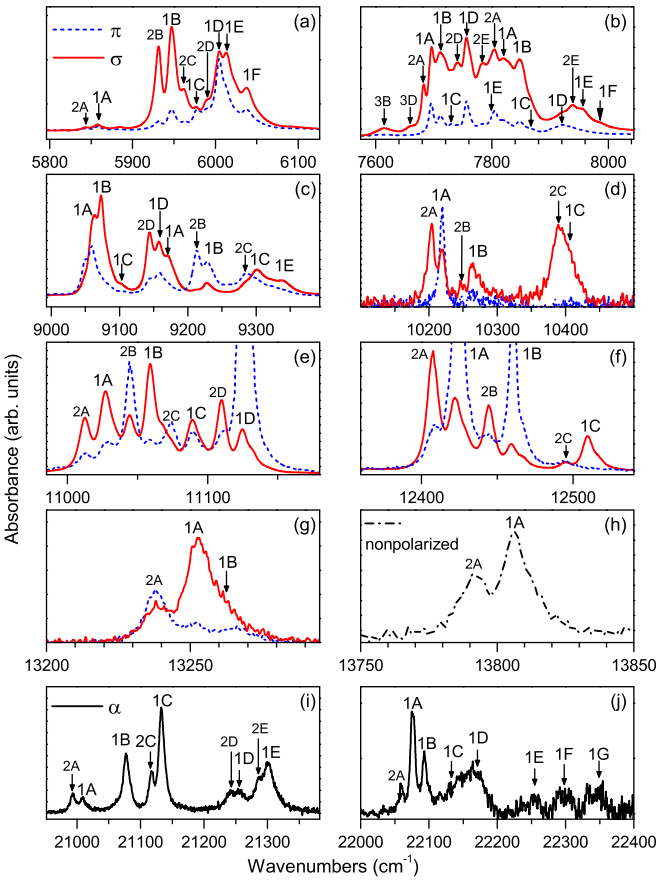

FIG. 4. Absorption spectra of $DyFe_3(BO_3)_4$ at the temperature 50 K in the σ (solid red lines), π (dashed blue lines), and α (solid black lines) polarizations, as well as in nonpolarized radiation (black dash-dot lines), corresponding to transitions from the lowest multiplet $^6H_{15/2}$ to sublevels of the excited multiplets (a) $^6H_{11/2}$, (b) $^6H_{9/2}$ and $^6F_{11/2}$, (c) $^6H_{7/2}$ and $^6F_{9/2}$, (d) $^6H_{5/2}$, (e) $^6F_{7/2}$, (f) $^6F_{5/2}$, (g) $^6F_{3/2}$, (h) $^6F_{1/2}$, (i) $^4F_{9/2}$, and (j) $^4I_{15/2}$.

from the lowest two sublevels of the multiplet $^6H_{15/2}$ separated by 15 cm^{-1} and populated at this temperature. The observed reversed intensities (Fig. 4) of the 1*X* and 2*X* (*X* = A, B, C, etc.) features for π- and σ-polarized incident radiation can be explained, at least qualitatively, by redistribution of intensities of the allowed electric dipole transitions from the two lowest Kramers doublets with close energies in the *R*32 phase (both with the Γ_4 symmetry in the trigonal CF, as follows from our CF calculations) between the 1*X* and 2*X* transitions in the CF of C_2 symmetry due to a specific structure of wave functions of the levels 1($^6H_{15/2}$) and 2($^6H_{15/2}$), which are orthogonal linear combinations of the wave functions of the Γ_4 doublets, and by relaxation of the selection rules of the D_3 point symmetry group in the C_2 group [$P3_121$ ($P3_221$) phase].

With increasing the temperature, spectral lines due to transitions from higher excited levels of the $^6H_{15/2}$ multiplet appear in the spectra. These lines are rather weak, and to improve signal to noise ratio, spectra at high temperatures were measured on the samples of larger thickness. The obtained energies of the excited CF sublevels of the multiplet $^6H_{15/2}$ are presented in Table I.

TABLE I. Crystal-field energies $E(\mathrm{cm}^{-1})$ of the Dy^{3+} ion in the paramagnetic ($T = 50$ K) phase of $DyFe_3(BO_3)_4$ determined from the analysis of the spectra and from calculations.

		E				E	
$^{2S+1}L_J$		Experiment	Theory	$^{2S+1}L_J$		Experiment	Theory
1		2	3	4		5	6
	1	0	0		A	9170	9161.4
	2	15	15.6	$^6F_{9/2}$	B	9228	9231.2
	3	97	94.5		C	9301	9298.8
$^6H_{15/2}$	4	186	191.4		D	–	9308.2
	5	228	231.5		E	9337	9333.2
	6	270	280.3		A	10219	10227
	7	335	345	$^6H_{5/2}$	B	10263.5	10273
	8	–	377.4		C	10406	10400
	A	3567	3571.4		A	11027.2	11033
	B	3579.6	3580.5		B	11059.2	11057
	C	3610	3608.5	$^6F_{7/2}$	C	11089.2	11071
$^6H_{13/2}$	D	3626.2	3633		D	11124.8	11098
	E	3688	3684.2		A	12422.3	12425
	F	3741	3732.6	$^6F_{5/2}$	B	12459.5	12455
	G	3782.7	3773.3		C	12509.6	12491
	A	5858	5860				
	B	5947	5951.6	$^6F_{3/2}$	A	13252.4	13246
$^6H_{11/2}$	C	5977.3	5976.8		B	13262.0[a]	13256
	D	6004.4	6008.4				
	E	6013	6015.7				
	F	6037.8	6044.1	$^6F_{1/2}$	A	13806.5	13800
	A	7696	7703.5		A	21008.6	21011
$^6H_{9/2}$	B	7711.3	7716.5	$^4F_{9/2}$	B	21077.3	21081
	C	7730	7732.9		C	21133	21100
	D	7756	7762.3		D	21255.0	21233
	E	7799	7807		E	21301	21244
	A	7820	7819.1		A	22075	22074
	B	7847	7839.6		B	22093	22092
$^6F_{11/2}$	C	7867	7877.7	$^4I_{15/2}$	C	22132	22139
	D	7921	7932.9		D	22168[a]	22203
	E	7954	7954		E	22254	22243
	F	7986	7976.2		F	22298	22284
					G	22348	22339
$^6H_{7/2}$	A	9062	9058.3		H	–	22375
	B	9073	9064.7				
	C	9102	9101.9				
	D	9158	9150.3				

[a]Line's position was specified consulting temperature-dependent spectra.

The optical multiplets measured in $DyFe_3(BO_3)_4$ with the low-temperature structure ($P3_121$ or $P3_221$) are similar to those measured in $YAl_3(BO_3)_4$ crystals (the $R32$ space group) containing impurity Dy^{3+} ions at Y^{3+} sites with the local D_3 symmetry [31–33]. However, the total splittings of the J multiplets in $DyFe_3(BO_3)_4$ are smaller than in $YAl_3(BO_3)_4$:Dy due to a more weak CF in dysprosium borate having larger lattice constants [$a = 0.95439$ and 0.92833 nm and $c = 0.75676$ and 0.72331 nm at room temperature in $DyFe_3(BO_3)_4$ [20] and $YAl_3(BO_3)_4$ [34,35], respectively]. Almost all the spectral lines observed in the transmission and absorption spectra of the paramagnetic phase of $DyFe_3(BO_3)_4$, in particular, at $T = 50$ K, were unambiguously identified, and the corresponding energies of excitations of the Dy^{3+} ions in the range 3500−22 400 cm^{-1} are given in Table I (columns 2 and 5). This dataset is a basis for the CF modeling described in the next section. Shifts and splittings of the spectral lines observed at temperatures below the magnetic ordering temperature $T_N = 39$ K will be discussed in a separate publication.

IV. DISCUSSION

A. The CF calculations for the $P3_121$ ($P3_221$) paramagnetic phase of $DyFe_3(BO_3)_4$

The primitive cell of the RE iron borate crystal lattice in the $P3_121$ (or $P3_221$) phase contains three formula units. Correspondingly, there are three crystallographically equivalent but magnetically nonequivalent RE ions with the local C_2 symmetry, connected by the $(2\pi/3)$ rotations around the c axis (see Fig. 1) and two types of nonequivalent helicoidal chains of the FeO_6 octahedra containing the Fe^{3+} ions at sites with the C_2 (Fe1) and C_1 (Fe2) local symmetries, respectively. The C_2 symmetry axes lie in the ab plane. In this paper, when analyzing spectral and static magnetic properties of $DyFe_3(BO_3)_4$, we assume that electrons are localized at the ions that form the crystal lattice and, following the approach used by us earlier in Refs. [24–26] and [36], start from a consideration of independent Dy^{3+} ions and dimers containing the nearest-neighbor iron ions $(Fe^{3+})_2$ in the chains coupled by the isotropic exchange. At this stage, all interactions between the ions, which involve dynamic electronic variables, even relative the time inversion, are considered in the framework of the CF approximation. A single Dy^{3+} ion and an iron dimer are described by the corresponding effective Hamiltonians. Further, the exchange interactions between the Fe^{3+} ions and between the Fe^{3+} and Dy^{3+} ions are taken into account in the framework of the self-consistent-field approximation.

The structure of the spectrum of an isolated Dy^{3+} ion with the ground $4f^9$ electronic configuration in a dielectric crystal can be described using the Hamiltonian

$$H_0 = H_{\mathrm{FI}} + H_{\mathrm{CF}}, \tag{1}$$

where

$$H_{\mathrm{FI}} = \zeta \sum_j \boldsymbol{l}_j \boldsymbol{s}_j + \alpha \hat{\boldsymbol{L}}^2 + \beta \hat{G}(G_2) + \gamma \hat{G}(R_7) + \sum_q (F^q \hat{f}_q + P^q \hat{p}_q + T^q \hat{t}_q + M^q \hat{m}_q) \tag{2}$$

is the free-ion Hamiltonian written in a standard form that includes the energies of the spin-orbit and electrostatic interactions between the $4f$ electrons and additional terms due to interconfigurational interactions [37]. The Hamiltonian H_{CF} stands for the energy of localized $4f$ electrons (labeled by the index j) in a static CF. Here, l_j and s_j are orbital and spin moments of electrons; $\hat{\boldsymbol{L}}$ is the total orbital moment; and the explicit forms of operators $\hat{G}, \hat{f}, \hat{p}, \hat{t}, \hat{m}$ are determined in literature (see references in Ref. [37]). In the present paper, we use parameters of the Hamiltonian [Eq. (2)] from

Ref. [35] for the impurity Dy^{3+} ions in $YAl_3(BO_3)_4$, slightly corrected to fit gaps between multiplet centers of gravity: $F^2 = 91\,060, F^4 = 63\,871, F^6 = 49\,460$, $\zeta = 1909$, $\alpha = 18$, $\beta = -633$, $\gamma = 1790$, $P^2 = 719, P^4 = 360, P^6 = 72, M^0 = 3.39, M^2 = 1.9, M^4 = 1.05, T^2 = 329, T^3 = 36, T^4 = 127$, $T^6 = -314, T^7 = 404, T^8 = 315$ (in cm^{-1}).

Let us introduce a local right-handed Cartesian system of coordinates with the origin at a selected Dy^{3+} ion and with the z_l axis along the crystallographic c axis and the x_l axis along the C_2 symmetry axis for the given site. In this local system of coordinates, the CF Hamiltonian for the Dy^{3+} ion is determined by fifteen real CF parameters B_q^p:

$$\begin{aligned} H_{CF} = \sum_{j=1}^{9} \{ & B_0^2 C_0^{(2)}(j) + B_0^4 C_0^{(4)}(j) + B_0^6 C_0^{(6)}(j) + i B_{-3}^4 \left[C_{-3}^{(4)}(j) + C_3^{(4)}(j)\right] + i B_{-3}^6 \left[C_{-3}^{(6)}(j) + C_3^{(6)}(j)\right] + B_6^6 \left[C_{-6}^{(6)}(j) + C_6^{(6)}(j)\right] \\ & + i B_{-1}^2 \left[C_{-1}^{(2)}(j) + C_1^{(2)}(j)\right] + B_2^2 \left[C_{-2}^{(2)}(j) + C_2^{(2)}(j)\right] + i B_{-1}^4 \left[C_{-1}^{(4)}(j) + C_1^{(4)}(j)\right] + B_2^4 \left[C_{-2}^{(4)}(j) + C_2^{(4)}(j)\right] \\ & + i B_{-1}^6 \left[C_{-1}^{(6)}(j) + C_1^{(6)}(j)\right] + B_2^6 \left[C_{-2}^{(6)}(j) + C_2^{(6)}(j)\right] + B_4^4 \left[C_{-4}^{(4)}(j) + C_4^{(4)}(j)\right] + B_4^6 \left[C_{-4}^{(6)}(j) + C_4^{(6)}(j)\right] \\ & + i B_{-5}^6 \left[C_{-5}^{(6)}(j) + C_5^{(6)}(j)\right] \}, \end{aligned} \tag{3}$$

where $C_q^{(p)}$ is the spherical tensor operator of the rank p, and the summation is over $4f$ electrons localized at the Dy^{3+} ion. Six parameters, namely, $B_0^2, B_0^4, B_{-3}^4, B_0^6, B_{-3}^6$, and B_6^6 in the first line of Eq. (3), define the dominant CF component of trigonal symmetry and other nine parameters define the CF component of the C_2 symmetry. The initial values of the CF parameters were calculated in the framework of the ECM [27]:

$$B_q^p = B_q^{(pc)p} + B_q^{(ec)p}. \tag{4}$$

The electrostatic field of point charges eq_L (e is the elemental charge) of lattice ions L with the spherical coordinates R_L, θ_L, φ_L (the origin of the coordinates is at the Dy^{3+} ion) is described by the parameters

$$\begin{aligned} B_q^{(pc)p} = & -\sum_L e^2 q_L (1-\sigma_p) \langle 4f|r^p|4f\rangle (-1)^q \\ & \times C_{-q}^{(p)}(\vartheta_L, \phi_L)/R_L^{p+1}, \end{aligned} \tag{5}$$

where σ_p are the shielding factors [38] and $-e\langle 4f|r^p|4f\rangle$ are the moments of the $4f$ electron charge distribution. The interaction of $4f$ electrons with the field of exchange charges defined through the overlap integrals $S_s(R_L) = \langle 4f0|2s\rangle, S_\sigma(R_L) = \langle 4f0|2p0\rangle$, $S_\pi(R_L) = \langle 4f1|2p1\rangle$ between the $4f$ wave functions ($|4f\, l_z\rangle$) of the Dy^{3+} ion and $2s$, and $2p$ wave functions of the electrons at the outer filled electronic shells of the nearest oxygen ions is described by the parameters

$$B_q^{(ec)p} = \sum_L \frac{2(2p+1)}{7} \frac{e^2}{R_L} S_p(R_L) (-1)^q C_{-q}^{(p)}(\vartheta_L, \phi_L). \tag{6}$$

In a general case, the model operates with three phenomenological parameters G_s, G_σ, G_π in the linear combinations of the squared overlap integrals

$$\begin{aligned} S_p(R_L) = & G_s [S_s(R_L)]^2 + G_\sigma [S_\sigma(R_L)]^2 \\ & + [2 - p(p+1)/12] G_\pi [S_\pi(R_L)]^2. \end{aligned} \tag{7}$$

The dependencies of the overlap integrals on the distance R (in Angstroms) between the ions, computed with the available radial wave functions of the Dy^{3+} [39] and O^{2-} [40] ions, can be approximated by the functions $S_u = a_u \exp(-b_u R^{c_u})$ ($u = s, \sigma$ and π), where $a_s = 0.26533, b_s = 0.859$, and $c_s = 1.5476$; $a_\sigma = 0.07039$, $b_\sigma = 0.2495$, and $c_\sigma = 2.2061$; $a_\pi = 1.40205$, $b_\pi = 2.2761$, and $c_\pi = 0.9358$.

In RE iron borates, interactions of RE ions with the nearest-neighbor oxygen ions bring the main contributions into the CF parameters. The lattice structure data for $DyFe_3(BO_3)_4$ were presented in Refs. [3,20]. In the $P3_121$ ($P3_221$) phase, the RE ions are at the $3a$ Wyckoff positions. Below, we use the same atomic notations as in Refs. [3,20] and consider explicitly the reference Dy^{3+} ion with the fractional coordinates $(-x_{Dy}, -x_{Dy}, 0)$. The nearest-neighbor six oxygen ions at the $6c$ Wyckoff sites O3, O4, and O7 form a deformed trigonal prism and can be divided into three pairs with fractional coordinates (x_{Oi}, y_{Oi}, z_{Oi}) and $(y_{Oi}, x_{Oi}, -z_{Oi})$ at the distances R(RE-Oi) from the RE ion ($i = 3, 4, 7$). As is seen in Table II, the distances between the Dy^{3+} and oxygen O3 and O4 ions presented in Ref. [20] contradict to trends in variations of these distances with the number of electrons in the $4f$ shell of a RE ion in other RE iron borates with the same structure. In the calculations described below, we use the structural data from Ref. [3] measured at the temperature 60 K, which seem to be more reliable. The transformation of x and y coordinates in the crystallographic trigonal frame presented in Ref. [3] to the Cartesian system of coordinates at the reference dysprosium site is defined by the equations

$$x_l = (x - y/2)\cos(\pi/3) + (\sqrt{3}y/2)\sin(\pi/3), \tag{8}$$

$$y_l = -(x - y/2)\sin(\pi/3) + (\sqrt{3}y/2)\cos(\pi/3). \tag{9}$$

TABLE II. Distances (in Angstroms) between the RE^{3+} ion and the neighbor oxygen ions in the $P3_121$ ($P3_221$) phase of RE iron borates.

Compound	T	R(RE-O3)	R(RE-O4)	R(RE-O7)	Ref.
$Gd(4f^7)Fe_3(BO_3)_4$	90 K	2.3485	2.3830	2.3474	[16]
$Tb(4f^8)Fe_3(BO_3)_4$	40 K	2.3147	2.3893	2.3598	[41]
$Dy(4f^9)Fe_3(BO_3)_4$	50 K	2.3725	2.3520	2.3474	[20]
$Dy(4f^9)Fe_3(BO_3)_4$	60 K	2.3353	2.3838	2.3280	[3]
$Ho(4f^{10})Fe_3(BO_3)_4$	50 K	2.3073	2.3938	2.3292	[42]

TABLE III. Crystal-field parameters B_q^p (cm^{-1}) for RE iron borates with the $P3_121$ structure. In the $P3_221$ structure, the parameters with $q = -1, -3$, and -5 have opposite signs.

p	q	$EuFe_3(BO_3)_4$ [43]	$TbFe_3(BO_3)_4$ [36]	$DyFe_3(BO_3)_4$ [Present paper]	
1		2	3	4	5
2	0	484	434	200[a]	404
4	0	–1255	–1256	–1255[a]	–1192
4	–3	619	608	539[a]	554.4
6	0	404	352	337[a]	328
6	–3	80	73	69[a]	70.3
6	6	290	270	203[a]	232
2	–1	39	38	66[a]	58.4
4	–1	–76	–66	–43[a]	–49.2
6	–1	–32	–27	–0.3[a]	–7.4
2	2	54	54	123[a]	69.4
4	2	102	82	104[a]	101.2
6	2	–11	–8	–13[a]	–14
4	4	–26	–23	16[a]	15.9
6	4	–31	–27	31[a]	31.4
6	–5	–131	–91	–92[a]	–79

[a]Parameters calculated by making use of the exchange-charge model.

The results of calculations of the CF parameters [Eq. (4)] performed in the framework of the simplest single-parameter version of ECM ($G_s = G_\sigma = G_\pi = 7.5$) are presented in Table III (column 4). The following values were used in calculations: $\langle r^2\rangle = 0.726, \langle r^4\rangle = 1.322$, and $\langle r^6\rangle = 5.107$ (in atomic units) [39]; $\sigma_2 = 0.646$ [38] and $\sigma_4 = \sigma_6 = 0$; $q_{Dy} = 3$, $q_{Fe} = 2$, $q_B = 2.25$, and $q_O = -1.5$ (the values of the ion charges). The obtained CF parameters correlate well with the results of similar calculations of the CF parameters for the Tb^{3+} ions in terbium iron borate [36] performed with the ECM parameters $G_s = G_\sigma = G_\pi = 7$, using the structure data from Ref. [41] for 40 K.

Next, the energies of transitions between the energy levels of the Dy^{3+} ions, obtained from the numerical diagonalization of the Hamiltonian [Eq. (1)] operating in the total space of 2002 states of the electronic $4f^9$ configuration, are compared with the measured optical spectra of $DyFe_3(BO_3)_4$ in the paramagnetic phase, and the initial CF parameters are varied to fit the experimental data. The final set of the CF parameters is presented in Table III (column 5), and the corresponding CF energies (columns 3 and 6 in Table I) match well the results of measurements (columns 2 and 5 in Table I). Note that values of the six CF parameters $B_0^2, B_0^4, B_{-3}^4, B_0^6, B_{-3}^6$, and B_6^6, which determine the trigonal component of the CF, change monotonically along the series of RE iron borates (in particular, CF parameters for the europium, terbium, and dysprosium compounds are compared in Table III; to add the data on Pr, Nd, and Sm compounds, see Table III of Ref. [26]). The remaining nine CF parameters of the C_2 symmetry CF component are determined with lower accuracy because of their relatively small influence on the multiplet splittings. However, only these nine CF parameters determine some specific properties of RE-iron borates in the $P3_121$ (or $P3_221$) phase, in particular, the anisotropy of the magnetic spectroscopic factors of Kramers doublets of the Dy^{3+} ions in the ab plane and the values of quadrupole moments that form right ($P3_121$) or left ($P3_221$) helixes in $DyFe_3(BO_3)_4$ [3].

B. Components of the g tensor for the Dy^{3+} ions, paramagnetic susceptibility of $DyFe_3(BO_3)_4$, and helix chirality of the local Dy^{3+} susceptibility

First, we discuss below peculiarities of the g tensor in the case of the low-symmetry $P3_121$ (or $P3_221$) phase. The effective spin-Hamiltonian for a Kramers doublet in a magnetic field $\boldsymbol{B}$ can be written as

$$H_S = \mu_B(g_1 S_1 B_1 + g_2 S_2 B_2 + g_3 S_3 B_3), \tag{10}$$

where μ_B is the Bohr magneton, B_α and S_α are projections of the magnetic field and effective spin moment ($S = 1/2$) on the principal axes of the tensor $G = g \cdot \tilde{g}$, and g_α are the square roots of the corresponding eigenvalues of this tensor. Components of the g tensor are determined by matrix elements of the magnetic moment operator of an ion, $\boldsymbol{m} = -\mu_B \sum_j (\xi \boldsymbol{l}_j + 2\boldsymbol{s}_j)$ (here ξ is the orbital reduction factor), in the basis of the wave functions $|\pm>$ of a Kramers doublet:

$$\begin{aligned} g_{\alpha x} &= 2\,\mathrm{Re}\langle +|m_\alpha|-\rangle/\mu_B, \\ g_{\alpha y} &= -2\,\mathrm{Im}\langle +|m_\alpha|-\rangle/\mu_B, \\ g_{\alpha z} &= 2\langle +|m_\alpha|+\rangle/\mu_B. \end{aligned} \tag{11}$$

In a CF of the C_2 symmetry, one of the principal axes is directed along the symmetry axis (i.e., the x_l axis in our case). From calculations performed in the basis of the eigenfunctions of the Hamiltonian [Eq. (1)], using the orbital reduction factor $\xi = 0.95$ (this value was found from the fit of the high-temperature magnetic susceptibilities, see below), we obtained the following principal values of the g tensors: $g_1 = g_{xx} = 0.072$ and 0.096, $g_2 = 0.005$ and 0.012, and $g_3 = 15.874$ and 14.369 for the ground and the first excited doublets of the Dy^{3+} ions in $DyFe_3(BO_3)_4$, respectively. Note that the calculated largest g factors (g_3) agree well with the measured g factors along the principal c axis $g_{cc} = 15.78$ and 12.03 of the ground and the first excited doublets (separated by a gap of about $3\,cm^{-1}$) of the impurity Dy^{3+} ions in $YAl_3(BO_3)_4$ with the $R32$ structure [44]. However, the principal axes corresponding to these largest g_3 factors in $DyFe_3(BO_3)_4$ are inclined from the c axis towards the y_l axis by the angles of 23.5° and 2.7° for the ground and the first excited doublets, respectively.

As a consequence, contrary to the RE iron (and aluminum) borates in the $R32$ phase, in paramagnetic borates with the $P3_121$ (or $P3_221$) structure, the external magnetic field parallel to the c axis induces not only longitudinal but also local transversal components of the magnetic moments; similarly, the magnetic field oriented in the ab plane induces local magnetic moments with projections on the c axis of different signs and values at different RE sites, depending on the angle between the field direction and the local C_2 axis.

Further, we calculate static magnetic susceptibilities $\chi_\parallel$ and $\chi_\perp$ of $DyFe_3(BO_3)_4$ single crystals for external magnetic fields parallel and perpendicular to the c axis, respectively, as functions of the temperature in a paramagnetic range $T_N < T < T_S$. In the paramagnetic phase, the renormalization of the susceptibility of the Fe^{3+} ions due to the f-d exchange interaction is rather weak (see Refs. [24,25], and [36]), and

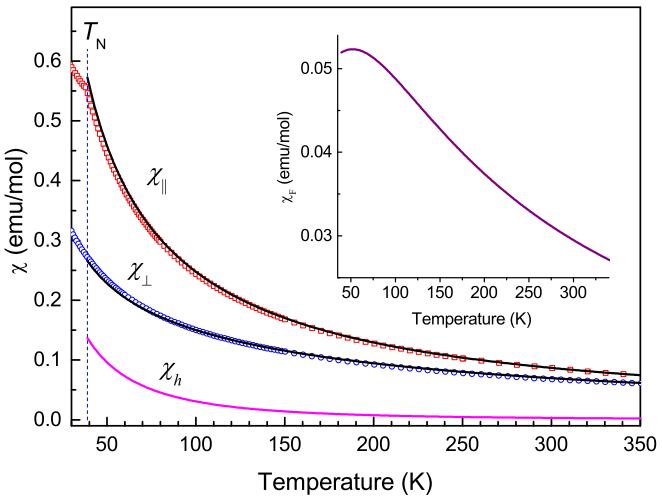

FIG. 5. Temperature dependencies of the longitudinal and transversal dc-susceptibilities of $DyFe_3(BO_3)_4$ measured in the external magnetic field $B = 0.05$ T [19] (symbols) and the helix single-site nondiagonal susceptibility of the Dy^{3+} ions. The results of calculations are represented by solid lines. The contribution of the iron subsystem into the total susceptibilities, $\chi_F = 3N_A\chi_{Fe}$, is shown in the inset.

we compare the sums of the computed susceptibilities of the independent RE and iron subsystems with the experimental data [19] in Fig. 5. It should be noted that we neglect here differences between the magnetic properties of the Fe1 and Fe2 ions. The principal axes of the susceptibility tensors of the three magnetically nonequivalent Dy^{3+} ions in the unit cell rotate around the c axis in accordance with the rotations of the local systems of coordinates introduced above. Correspondingly, all the ions have the same projections of their magnetic moments on the external field parallel to the c axis, and $\chi_{||} = N_A(\chi_{Dy,zz} + 3\chi_{Fe})$, where N_A is the Avogadro number. The transversal component of the bulk susceptibility tensor is written as follows: $\chi_\perp = N_A[(\chi_{Dy,xx} + \chi_{Dy,yy})/2 + 3\chi_{Fe}]$. The effective isotropic susceptibility χ_{Fe} of an iron ion was calculated using the analytical expression derived in the framework of the dimer model [see eqs. (8)–(10) in Ref. [24]]. We employed the values of the exchange integrals $J_{nn} = -8$ K and $J_{nnn} = -2.5$ K for the nearest-neighbor and next-nearest-neighbor antiferromagnetic interactions between the iron ions within the chains and in the neighboring chains, respectively, which are slightly larger than the obtained earlier exchange integrals in terbium and samarium iron borates [26,36] due to shorter distances between the ions in dysprosium iron borate. The temperature dependence of the contribution of the iron subsystem into the bulk susceptibilities is shown in the inset of Fig. 5. The components of the susceptibility tensor $\chi_{Dy,\alpha\beta} = \langle m_\alpha\rangle/B_\beta$ for a single Dy^{3+} ion were obtained vs temperature with a step of one K from numerical simulations of average values of magnetic moment components m_α induced by external magnetic fields B_β ($B_\beta = 0.1$ T) using the equilibrium density matrix defined by the Hamiltonian $H_0 - m_\beta B_\beta$. A good agreement between the calculated and measured temperature dependencies of the longitudinal and transversal susceptibilities (see Fig. 5) testifies a reliability of the parameters derived in the present paper.

TABLE IV. Quadrupole moments of the Dy^{3+} ions in the $P3_121$ phase of $DyFe_3(BO_3)_4$.

	$\langle Q_{x_l^2-y_l^2}\rangle$		$\langle Q_{y_lz_l}\rangle/\langle Q_{x_l^2-y_l^2}\rangle$	
Temperature	Measured [3][a]	Computed[b]	Measured [3]	Computed
50 K	–1.22	–1.18	–1.23	–1.415
100 K	–0.906	–0.906	–1.20	–1.202
150 K	–0.678	–0.695	–1.10	–1.096
200 K	–0.50	–0.548	–0.90	–1.031

[a]Arbitrary units.
[b]The absolute values are scaled to match the measured value at $T =$ 100 K.

The helix chirality of the local susceptibility can be characterized by a nondiagonal component $\chi_{Dy,yz}$ of the susceptibility of a single Dy^{3+} ion. It determines a projection of the dysprosium magnetic moment on the ab plane, induced by a magnetic field directed along the c axis. This in-plane component of the dysprosium magnetic moment rotates around the magnetic field $\boldsymbol{B}||c$ in a clockwise (counterclockwise) direction in the $P3_121$ ($P3_221$) phase. The susceptibility $\chi_h = N_A\chi_{Dy,yz}$ is compared with $\chi_{||}$ and $\chi_\perp$ in Fig. 5. The helix chirality of the local susceptibility tensor, inaccessible by macroscopic magnetometry on single crystals, could be detected in polarized neutron diffraction [45] or resonant x-ray magnetic scattering [46,47] experiments on paramagnetic $DyFe_3(BO_3)_4$ subjected to a magnetic field directed along the c axis.

C. Quadrupole moments of Dy^{3+} in the $P3_121$ ($P3_221$) phase

The low-symmetry CF C_2 component distorts the electronic density distribution in the Dy^{3+} ions and induces nonzero components of the quadrupole moment, in particular, $Q_{x_l^2-y_l^2} = \sum_j [C_2^{(2)}(j) + C_{-2}^{(2)}(j)]/2$ and $Q_{y_lz_l} = -i\sum_j [C_1^{(2)}(j) + C_{-1}^{(2)}(j)]/2$ (in units of $e\langle r^2\rangle$) at the reference dysprosium site [48,49]. The quadrupole helix chirality appears due to rotations of the local C_2 symmetry axis by $2\pi/3$ and $4\pi/3$ at the $3a$ dysprosium sites shifted relative one another along the c axis by $c/3$ and $2c/3$, respectively. The results of calculations of the average values of the quadrupole moment components,

$$\langle Q\rangle = \mathrm{Tr}[Q\exp(-H_0/k_BT)]/\mathrm{Tr}[\exp(-H_0/k_BT)], \quad (12)$$

at different temperatures T (k_B is the Boltzmann constant) using the final set of the CF parameters from column 5 in Table III in the single-ion Hamiltonian [Eq. (1)] agree satisfactorily with the experimental data presented in Ref. [3] (see Table IV) and confirm a supposition made in Ref. [3] that changes of $\langle Q_{x_l^2-y_l^2}\rangle$ and $\langle Q_{y_lz_l}\rangle$ with temperature are induced, mainly, by a redistribution of population between CF sublevels of the lowest multiplet $^6H_{15/2}$ of the Dy^{3+} ion.

V. CONCLUSION

To summarize, we have performed a high-resolution polarized temperature-dependent optical spectroscopy and theoretical studies of $DyFe_3(BO_3)_4$ single crystals. Those are crystals in which a new effect of "chirality of electronic

quadrupole moments" was observed in RXD studies using circularly polarized x rays [3]. This quadrupole chirality, as well as chirality of transverse magnetic moments induced by an external longitudinal magnetic field $\boldsymbol{B}||c$ in the RE iron borates with the $P3_121$ (or $P3_221$) structure, is caused by a specific geometry of the crystal lattice containing helical iron chains propagating along the c axis (these chains are present also in the high-temperature $R32$ phase and cause a crystallographic chirality) and three magnetically nonequivalent RE ions in the CFs rotating by $2\pi/3$ around the c axis. Whereas the crystallographic chirality can be detected by optical activity measurements, to probe experimentally the chirality of multipole moments, such as magnetic dipoles and electric quadrupoles, one has to use a method with a space resolution at the nanoscopic length scale comparable to dimensions of the unit cell. Studies of the angular dependencies of the resonant x-ray scattering allow one to obtain information about a space inhomogeneity of the electronic shells of Dy^{3+} ions [3]; however, widths of corresponding spectral envelopes exceed by orders of magnitude the CF splittings of the multiplets of the ground electronic $4f^9$ configuration. The energetic analysis based on the measurements of frequencies of f-f transitions in Dy^{3+} ions provides no information on the helicity, but it reveals a complete set of CF parameters. The low-symmetry CF component distorts the electronic density distribution in the Dy^{3+} ions and induces nonzero components of the quadrupole moment and an anisotropy of the magnetic spectroscopic factors of Kramers doublets of the Dy^{3+} ions in the ab plane. The low-symmetry CF parameters for the Dy^{3+} ion in the $P3_121$ ($P3_221$) phase, obtained from the CF calculations performed on the basis of the spectral data, give possibility to calculate explicitly the values of the components of the electronic quadrupole moment, while only the relative values of these components can be obtained from angular variations of the RXD [3]. Thus, measurements of the RXD (allowing to distinguish contributions into the structure factor from different RE ions in the unit cell) and a conventional optical spectroscopy (complemented by an analysis of the measured CF splittings with taking into account the real geometry of the RE surroundings) are mutually complementary methods of chirality studies. Our paper elucidates a physical reason of appearance of RE in-plane quadrupole moments below the temperature T_S of the structural phase transition $R32$ - $P3_121$ ($P3_221$). The single-site magnetic susceptibility tensors of the magnetically nonequivalent Dy^{3+} ions also have a property of helix chirality. As follows from calculations, transversal and longitudinal components of the dysprosium magnetic moment in an external magnetic field parallel to the c axis have comparable values. The longitudinal magnetization is measured by a conventional magnetometric technique, but the transversal magnetization, being a geometric sum of contributions connected by the $(2\pi/3)$ rotations around the c axis, equals zero. However, we suggest that the components of the Dy^{3+} single-ion magnetic moments in the ab plane, which rotate around the c axis, can be revealed by polarized neutron or resonant x-ray scattering experiments in a magnetic field.

ACKNOWLEDGMENTS

This paper was supported by the Russian Scientific Foundation (Grant No. 14-12-01033). I.A.G. thanks L. N. Bezmaternykh for useful comments concerning the crystal growth and the Russian Foundation for Basic Research for financial support under Grant No. 14-02-00307a.

[1] E. U. Condon, Rev. Mod. Phys. **9**, 432 (1937).
[2] S.-W. Cheong and M. Mostovoy, Nat. Mater. **6**, 13 (2007).
[3] T. Usui, Y. Tanaka, H. Nakajima, M. Taguchi, A. Chainani, M. Oura, S. Shin, N. Katayama, H. Sawa, Y. Wakabayashi, and T. Kimura, Nat. Mater. **13**, 611 (2014).
[4] J. C. Joubert, W. B. White, and R. J. Roy, J. Appl. Cryst. **1**, 318 (1968).
[5] E. Bovero, Z. D. Luo, Y. D. Huang, A. Benayas, and D. Jaque, Appl. Phys. Lett. **87**, 211108 (2005).
[6] J. M. Dawes, P. Dekker, Ph. Burns, and J. A. Piper, Opt. Rev. **12**, 101 (2005).
[7] K. N. Gorbachenya, V. E. Kisel, A. S. Yasukevich, V. V. Maltsev, N. I. Leonyuk, and N. V. Kuleshov, Opt. Lett. **41**, 918 (2016).
[8] A. K. Zvezdin, S. S. Krotov, A. M. Kadomtseva, G. P. Vorob'ev, Yu. F. Popov, A. P. Pyatakov, L. N. Bezmaternykh, and E. A. Popova, JETP Lett. **81**, 272 (2005).
[9] R. P. Chaudhury, F. Yen, B. Lorenz, Y. Y. Sun, L. N. Bezmaternykh, V. L. Temerov, and C. W. Chu, Phys. Rev. B **80**, 104424 (2009).
[10] A. M. Kadomtseva, G. P. Vorob'ev, Yu. F. Popov, A. P. Pyatakov, A. A. Mukhin, V. Yu. Ivanov, A. K. Zvezdin, I. A. Gudim, V. L. Temerov, and L. N. Bezmaternykh, JETP **114**, 810 (2012).
[11] T. Kurumaji, K. Ohgushi, and Y. Tokura, Phys. Rev. B **89**, 195126 (2014).
[12] R. P. Chaudhury, B. Lorenz, Y. Y. Sun, L. N. Bezmaternykh, V. L. Temerov, and C. W. Chu, Phys. Rev. B **81**, 220402(R) (2010).
[13] K.-C. Liang, R. P. Chaudhury, B. Lorenz, Y. Y. Sun, L. N. Bezmaternykh, V. L. Temerov, and C. W. Chu, Phys. Rev. B **83**, 180417(R) (2011).
[14] A. M. Kadomtseva, Yu. F. Popov, G. P. Vorob'ev, N. V. Kostyuchenko, A. I. Popov, A. A. Mukhin, V. Yu. Ivanov, L. N. Bezmaternykh, I. A. Gudim, V. L. Temerov, A. P. Pyatakov, and A. K. Zvezdin, Phys. Rev. B **89**, 014418 (2014).
[15] N. V. Volkov, I. A. Gudim, E. V. Eremin, A. I. Begunov, A. A. Demidov, and K. N. Boldyrev, JETP Lett. **99**, 67 (2014).
[16] S. A. Klimin, D. Fausti, A. Meetsma, L. N. Bezmaternykh, P. H. M. van Loosdrecht, and T. T. M. Palstra, Acta Crystallogr. Sect. B: Struct. Sci. **61**, 481 (2005).
[17] D. Fausti, A. A. Nugroho, P. H. M. van Loosdrecht, S. A. Klimin, M. N. Popova, and L. N. Bezmaternykh, Phys. Rev. B **74**, 024403 (2006).
[18] Y. Hinatsu, Y. Doi, K. Ito, M. Wakeshima, and A. Alemi, J. Solid State Chem. **172**, 438 (2003).
[19] E. A. Popova, N. Tristan, A. N. Vasiliev, V. L. Temerov, L. N. Bezmaternykh, N. Leps, B. Buchner, and R. Klingeler, Eur. Phys. J. B **62**, 123 (2008).
[20] C. Ritter, A. Pankrats, I. Gudim, and A. Vorotynov, J. Phys.: Conf. Series **340**, 012065 (2012).

[21] Yu. F. Popov, A. P. Pyatakov, A. M. Kadomtseva, G. P. Vorob'ev, A. K. Zvezdin, A. A. Mukhin, V. Yu. Ivanov, and I. A. Gudim, J. Exp. Theor. Phys. **111**, 199 (2010).
[22] A. V. Malakhovskii, A. L. Sukhachev, A. Yu. Strokova, and I. A. Gudim, Phys. Rev. B **88**, 075103 (2013).
[23] D. V. Volkov, A. A. Demidov, and N. P. Kolmakova, J. Exp. Theor. Phys. **106**, 723 (2008).
[24] M. N. Popova, E. P. Chukalina, T. N. Stanislavchuk, B. Z. Malkin, A. R. Zakirov, E. Antic-Fidancev, E. A. Popova, L. N. Bezmaternykh, and V. L. Temerov, Phys. Rev. B **75**, 224435 (2007).
[25] M. N. Popova, T. N. Stanislavchuk, B. Z. Malkin, and L. N. Bezmaternykh, Phys. Rev. B **80**, 195101 (2009).
[26] M. N. Popova, E. P. Chukalina, B. Z. Malkin, D. A. Erofeev, L. N. Bezmaternykh, and I. A. Gudim, J. Exp. Theor. Phys. **118**, 111 (2014).
[27] B. Z. Malkin, Ion-phonon interactions, in *Spectroscopic Properties of Rare Earths in Optical Materials*, Vol. 83, edited by G. Liu and B. Jacquier, Springer Series in Materials Science (Tsinghua University Press and Springer-Verlag, Berlin, 2005), pp. 130–190.
[28] I. A. Gudim, A. I. Pankrats, E. I. Durnaikin, G. A. Petrakovskii, L. N. Bezmaternykh, R. Szymczak, and M. Baran, Crystallogr. Rep. **53**, 1140 (2008).
[29] L. N. Bezmaternykh, V. L. Temerov, I. A. Gudim, and N. A. Stolbovaya, Crystallogr. Rep. **50**, S97 (2005).
[30] S. A. Klimin, A. B. Kuzmenko, M. A. Kashchenko, and M. N. Popova, Phys. Rev. B **93**, 054304 (2016).
[31] G. Dominiak-Dzik, P. Solarz, W. Ryba-Romanowski, E. Beregi, and L. Kovacs, J. Alloys Compd. **359**, 51 (2003).
[32] E. Cavalli, E. Bovero, N. Magnani, M. O. Ramirez, A. Speghini, and M. Bettinelli, J. Phys.: Condens. Matter **15**, 1047 (2003).
[33] A. Baraldi, R. Capeletti, N. Magnani, M. Mazzera, E. Beregi, and I. Foldvari, J. Phys.: Condens. Matter **17**, 6245 (2005).
[34] E. L. Belokoneva, A. V. Azizov, N. I. Leonyuk, M. A. Simonov, and N. V. Belov, J. Struct. Chem. **22**, 476 (1981).
[35] C. Gorller-Warland, P. Vandevelde, and I. Hendrickx, Inorg. Chim. Acta **143**, 259 (1988).
[36] M. N. Popova, T. N. Stanislavchuk, B. Z. Malkin, and L. N. Bezmaternykh, J. Phys.: Condens. Matter **24**, 196002 (2012).
[37] W. T. Carnall, G. L. Goodman, K. Rajnak, and R. S. Rana, J. Chem. Phys. **90**, 3443 (1989).
[38] R. P. Gupta and S. K. Sen, Phys. Rev. A **7**, 850 (1973).
[39] A. J. Freeman and R. E. Watson, Phys. Rev. **127**, 2058 (1962).
[40] E. Clementi and A. D. McLean, Phys. Rev. **133**, A419 (1964).
[41] C. Ritter, A. Balaev, A. Vorotynov, G. Petrakovskii, D. Velikanov, V. Temerov, and I. Gudim, J. Phys.: Condens. Matter **19**, 196227 (2007).
[42] C. Ritter, A. Vorotynov, A. Pankrats, G. Petrakovskii, V. Temerov, I. Gudim, and R. Szymczak, J. Phys.: Condens. Matter **20**, 365209 (2008).
[43] M. N. Popova, B. Z. Malkin, K. N. Boldyrev, T. N. Stanislavchuk, D. A. Erofeev, V. L. Temerov, and I. A. Gudim, Phys. Rev. B **94**, 184418 (2016).
[44] A. D. Prokhorov, A. A. Prokhorov, E. E. Zubov, L. F. Chernysh, V. Dyakonov, and H. Szymczak, Low Temp. Phys. **40**, 730 (2014).
[45] H. B. Cao, A. Gukasov, I. Mirebeau, P. Bonville, C. Decorse, and G. Dhalenne, Phys. Rev. Lett. **103**, 056402 (2009).
[46] H. Mo, Ch. S. Nelson, L. N. Bezmaternykh, and V. T. Temerov, Phys. Rev. B **78**, 214407 (2008).
[47] J. Fink, E. Schierle, E. Weschke, and J. Geck, Rep. Prog. Phys. **76**, 056502 (2013).
[48] S. W. Lovesey, E. Balcar, K. S. Knight, and J. Fernandez Rodriguez, Physics Reports **411**, 233 (2005).
[49] S. W. Lovesey, E. Balcar, and Y. Tanaka, J. Phys. Condens. Matter **20**, 272201 (2008).